

# Characterization of Dynamic Friction in MEMS-Based Microball Bearings

Ta-Wei Lin, Alireza Modafe, *Student Member, IEEE*, Benjamin Shapiro, and Reza Ghodssi, *Member, IEEE*

**Abstract**—Rolling element bearing is a well-known concept in macroscale machinery applications. They are prospective candidates for friction reduction in microelectromechanical system (MEMS), as well as for providing stable, robust support for moving micromechanisms. The characteristics of rolling element bearings need to be investigated to facilitate their applications in MEMS. It is well understood that the measured data on the macroscale cannot be directly applied to the microscale. This paper presents an *in-situ* noncontact experimental system to characterize the friction behavior of microball bearings on the microscale. The methodology presented in this paper provides a useful template to study the dynamical behavior of linear microball bearings with a variety of materials, geometries, and surface qualities. The system, actuated by a motor, affords wide ranges of motion for measuring the dynamic friction using a vision system. It allows the determination of the coefficient of friction (COF) without any interference due to the measurement system. With careful optimization, the error in measurement has been reduced to 2%. Different designs of microball bearings are proposed to achieve lower friction. The studied microball bearings demonstrated an average static COF of 0.01 and an average dynamic COF of 0.007 between stainless-steel and silicon-micromachined contacting surfaces at 27 °C and 40% relative humidity.

**Index Terms**—Microelectromechanical systems (MEMS), microball bearings, rolling friction, silicon micromachining, V-grooves.

## I. INTRODUCTION

**F**RICITION is inevitable in mechanisms where components in contact have relative motion. The effects of friction become increasingly significant as the system size shrinks. Therefore, friction becomes critical on the microscale and is one of the fundamental limitations in the design and implementation of reliable, efficient MEMS devices like micromotors, microgenerators, and microengines.

Since the advent of the first micromotors in the late 1980s [1], [2], various types of actuation mechanisms have been reported for micromachines. Although much work has been

dedicated to MEMS reliability [3]–[6], there remains insufficient understanding of friction, wear, and other reliability related phenomena in microelectromechanical devices. Several different bearing and support structures were demonstrated for use in micromachines based on two categories: contact-type and noncontact-type. Previous contact-type bearings, like center-pin bearing with sliding bushings as support in the early polysilicon surface-micromachined micromotors [7], [8] suffered drastically from friction and wear. The friction and wear problems were less in wobble [9] and conical [10] micromotors, however, with a downfall in rotation speed. Noncontact-type bearings with more complicated support mechanisms like electrostatic [11] and pressurized air [12] levitation schemes have also been investigated. They show much less friction and almost no wear compared to contact-type bearings, with two major drawbacks: fabrication complexity and rotor instability. Among the contact-type bearings, ball bearing seems promising for future micromachinery applications due to the fact that 1) the bearing mechanism is relatively simple, 2) the rolling motion of the balls exhibits much less friction than sliding motion of other contact-type bearings, and 3) the balls provide a stable and robust support for the rotor. Linear microball bearings may be used in applications such as precision, long-range XY micropositioners for optical alignment or storage devices. Rotary microball bearings have applications in high-power microturbomachines such as micromotors, micropumps, microcoolers, microcompressors, and electrical power microgenerators. However, the behavior of ball bearings on the microscale needs to be investigated and characterized in order to utilize the microball bearings as an enabling tool in MEMS.

A linear microball bearing structure was proposed by Ghodssi *et al.* [13] to alleviate the effects of friction. Here, the gap between two moving and stationary plates was maintained by aligned silicon-micromachined V-grooves and stainless-steel microballs. Ghodssi tilted the plates to cause the onset of motion due to gravity. This was used to characterize the friction behavior of the bearings. Only the static coefficient of friction (COF) could be studied by this method. The static COF between silicon V-groove walls and stainless-steel microballs was reported as low as 0.056 (without load). In order to facilitate applications in MEMS, the whole friction characteristics (both static and dynamic) must be investigated.

Several approaches have been proposed to study the friction on the nano- and microscale including atomic force and friction force microscopes (AFM and FFM) [14]–[21], non-AFM/FFM methods [22]–[28], and *in-situ* direct measurement using micromachined structures [29]–[33]. It is well understood

Manuscript received May 6, 2003, revised January 21, 2004. This work was supported in part by the National Science Foundation under Grant ECS-0224361.

T.-W. Lin was with the Department of Electrical and Computer Engineering and the Institute for Systems Research, University of Maryland, College Park, MD 20742 USA. He is now with Asia Pacific Microsystems, Inc., Hsinchu, Taiwan 300, R.O.C.

A. Modafe and R. Ghodssi are with the Department of Electrical and Computer Engineering and the Institute for Systems Research, University of Maryland, College Park, MD 20742 USA (e-mail: ghodssi@eng.umd.edu).

B. Shapiro is with the Department of Aerospace Engineering and the Institute for Systems Research, University of Maryland, College Park, MD 20742 USA (e-mail: benshap@eng.umd.edu).

Digital Object Identifier 10.1109/TIM.2004.827089

that frictional behavior and appropriate models to describe this behavior are intimately linked to time and length scales, which have been categorized in five hierarchy levels: quantum, atomic, microstructural, continuum, and engineering design models [34]. As the referenced literature suggests, there has been a significant amount of experimental approaches for investigation of friction in short and long length-time scale levels. However, measurements taken on the nanoscale do not translate into reliable friction information on the microscale. Most MEMS applications lie in microstructural level where further research on modeling and experimental techniques is needed. In addition, almost all of the above mentioned methods were designated to study sliding friction, not rolling friction.

In this paper, we designed and built an *in-situ*, noncontact measurement system to characterize the dynamic friction of linear microball bearings. The measurement system is based on the measurement of displacement. There are number of methods for displacement sensing in MEMS, such as optical techniques and laser interferometry [35], [36] and capacitive sensing methods [37]. An alternative method is to measure the acceleration directly using an accelerometer. However, our choice of the measurement method was based on the following considerations: 1) most optical equipment and laser interferometers are expensive, 2) range of displacement in MEMS integrated displacement sensors like capacitive sensors is limited, 3) additional fabrication steps in preparing the test samples should be avoided as much as possible, 4) test setup should not interfere with the motion, and 5) flexibility and expandability of the measurement system are important. The frictional behavior of microball bearings has been successfully explored using the proposed system. We also demonstrated relatively low static and dynamic friction of a microball bearing design. The collected data can provide a basis for design and use of microball bearings in MEMS devices and systems.

## II. MICROBALL BEARINGS

A schematic view of a linear microball bearing is shown in Fig. 1. Parallel V-grooves are etched on only one side of two identical silicon plates ( $10\text{ mm} \times 10\text{ mm} \times 500\text{ }\mu\text{m}$ ) from a (100) silicon wafer. Equal numbers of precision microballs (Thomson Precision, Bristol, CT) are placed in each V-groove of the bottom plate (stator). The V-grooves of the top plate (slider) are aligned to those of the stator where they rest on the microballs. Only the walls of the V-grooves on both plates are in contact with the microballs.

The microballs in this study are made of stainless steel 440 C with a diameter of  $285\text{ }\mu\text{m}$  and a grade of 10 (see Table I for grade ten specifications). However, microballs as small as  $150\text{ }\mu\text{m}$  in diameter and as precise as grade 3 are available off-the-shelf. The  $285\text{-}\mu\text{m}$  microballs are big enough to be handled by a tweezers, but still small enough to exhibit the microscale behavior of friction. Furthermore, the dimensions of the V-grooves ( $300\text{ }\mu\text{m}$  in width and  $150\text{ }\mu\text{m}$  in depth) and the diameter of the microballs is chosen to maintain a  $70\text{-}\mu\text{m}$  gap between the slider and the stator, as shown in Fig. 2. The walls of the V-grooves have an angle of  $54.7^\circ$  with the bottom

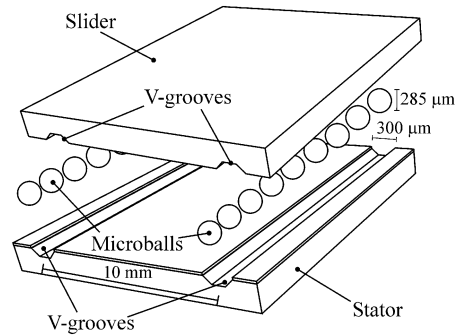


Fig. 1. Schematic diagram of microball bearings.

TABLE I  
SPECIFICATIONS OF GRADE 10 AMERICAN BALL  
MANUFACTURERS ASSOCIATION (ABMA) STANDARD

Specification	Value
Grade	10
Size Range	$152.4\text{ }\mu\text{m}$ to $22225\text{ }\mu\text{m}$
Deviation from Spherical Form	$0.254\text{ }\mu\text{m}$
Lot Diameter Variation	$\pm 0.254\text{ }\mu\text{m}$
Allowable Ball Gage Variation	$\pm 1.27\text{ }\mu\text{m}$
Maximum Surface Roughness	$25.4\text{ nm}$

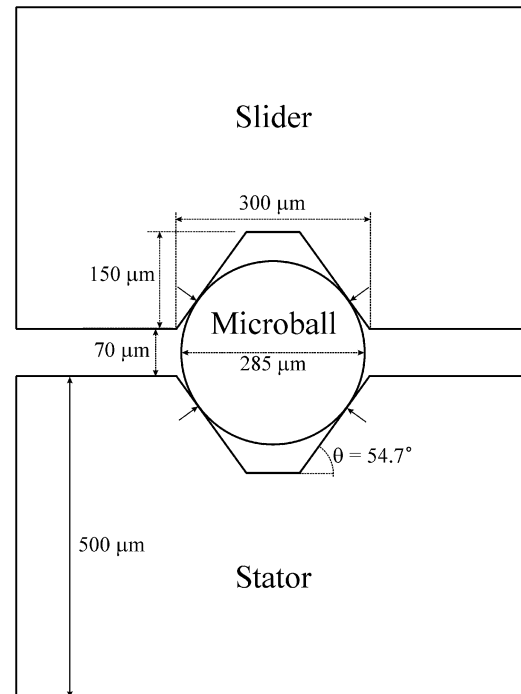


Fig. 2. Schematic cross section of V-grooves and a microball. Arrows show the contact points between the stator/slider and the microball, where the friction forces are applied. The dimensions are to scale.

surface due to the crystal orientation of (100) and (111) planes in the silicon wafer.

A silicon micromachining process [38] was developed and implemented to achieve the critical dimensions of the silicon V-grooves. The slider and the stator were fabricated from a  $4''$  silicon wafer with a  $3000\text{ }\text{\AA}$  low-stress silicon nitride layer on both sides. The wafer was cleaned using standard RCA procedure. The V-groove etch mask was then patterned using a standard photolithography process with a contact mask aligner. No

alignment marks were etched before patterning the etch mask, instead the V-groove patterns on the optical mask were carefully aligned parallel to the flat of the wafer. A plasma etch with tetrafluoromethane ( $\text{CF}_4$ ) gas was then used to etch the silicon nitride layer to form the V-groove etch mask. The wafer was immersed into a 1: 10 HF solution for 30 s to remove the native oxide from the exposed silicon surfaces. Finally, the wafer was put into a 45% (by weight) potassium hydroxide (KOH) solution at 60 °C for 9 h (without agitation). The etching apparatus sits inside a temperature-controlled bath with a reflux condenser to keep the concentration of the KOH solution constant. The average etch rate is about 16.7  $\mu\text{m}/\text{h}$ . The measured depth of the V-groove is 150  $\mu\text{m}$ .

### III. EXPERIMENTAL SYSTEM

When the stator oscillates in the direction parallel to the V-grooves, the microballs roll along the V-groove due to the friction at the contact points between the balls and the V-groove walls of the stator. Once the microballs move, the friction at contact points between the balls and the V-groove walls of the stator will introduce a force on the slider and cause it to have a velocity  $v'$ ; and acceleration  $a'$ . The COF is simply the ratio of the tangential force and the normal force applied at the contact point between the microballs and the V-groove walls. The tangential force is proportional to  $a'$  and the normal force is proportional to  $g/\cos\theta$ , where  $g$  is the acceleration due to gravity, and  $\theta$  is the angle between (100) and (111) planes in crystalline silicon equal to 54.7°. Therefore, if the acceleration  $a'$  of the slider can be measured, then  $\mu_r$ , the instantaneous COF of the stainless steel/silicon surface will be

$$\mu_r = \left(\frac{a'}{g}\right) \cos\theta. \quad (1)$$

An experimental system consisting of an actuation mechanism and a vision subsystem is designed and realized to generate the linear oscillation of the microball bearing and to measure the acceleration of the slider. The schematic diagram of the system is shown in Fig. 3. The actual built setup is shown in Figs. 4 and 5. It consists of a servomotor, linkages, a sliding platform, smooth rails, a CCD camera, and a linear microball bearing.

A “crank and slider” mechanism, as seen in Fig. 4, is applied to accomplish the oscillatory motion. A 14 × 14 × 1 cm platform is attached to four Thomson Super Ball Bushing open pillow blocks to enforce a smooth oscillatory motion. These blocks are installed on two 1.27 × 30.48 cm sliding rails. The rails are positioned parallel to each other so that the platform and pillow blocks assembly can slide smoothly along the rails. The platform is connected to a 30 × 1.9 × 0.96 cm aluminum bar (linkage 2). This is, in turn, connected to a 20-cm aluminum extrusion bar (linkage 1) using a small 3.1 × 4.1 × 1 cm aluminum block. The block can slide along the slot on the extrusion bar. By changing the position of the small block on the extrusion bar one can vary  $l_1$ , the length of linkage 1. The middle of the aluminum extrusion bar is fixed to the shaft of a dc servomotor. The motor used in this system is a SmartMotor SM2310 servomotor (Animatics Corporation, Santa Clara, CA). The motor is

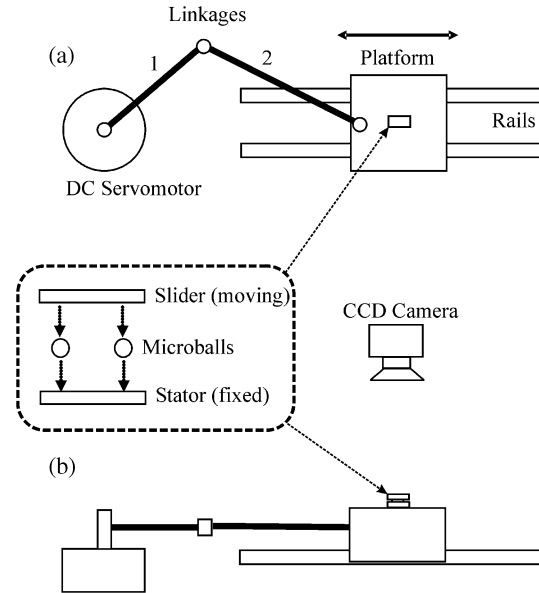


Fig. 3. Schematic of the experimental setup used to characterize the friction behavior of the microball bearings. (a) Top view as seen from the CCD camera. (b) Side view.

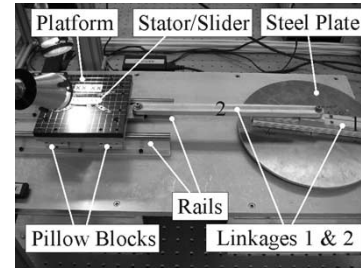


Fig. 4. Actuation mechanism: crank, slider mechanism, and oscillating platform. A dc servomotor is located underneath the aluminum template.

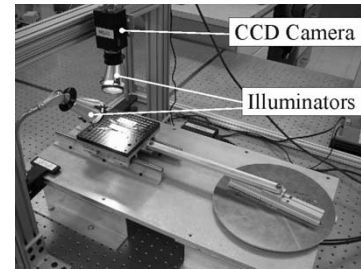


Fig. 5. Complete experimental setup, including the vision subsystem, installed on an antivibration air table. The camera and illuminators are installed right above the oscillating platform.

integrated with a PID controller. The speed, acceleration, and displacement can all be controlled from a PC-based software such as SMI (Animatics, Santa Clara, CA) or LabVIEW (National Instruments, Austin, TX). A 25-cm diameter steel plate with a thickness of 0.5 cm is attached under the aluminum extrusion bar to increase the rotation inertia of the linkage mechanism. This is done to smooth out the motion jitters due to the interaction of the control system with the friction inside the motor and the friction inside the pillow blocks. The motor combined with the linkages causes the platform to undergo a smooth linear oscillatory motion along the precisely machined rails. The stator

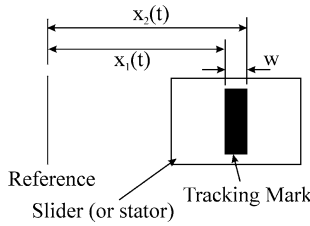


Fig. 6. Tracking mark on the slider (or stator) and the reference.

is attached to the top surface of the sliding platform by clamps on all four edges.

A Vision 1400 system (National Instruments, Austin, TX) is used for image recording and processing in this experiment. The system includes a JAI CV-M50 CCD camera, a PCI-1408 frame grabber, and IMAQ Vision Builder software. The camera has a maximum  $640 \times 480$  dpi resolution and 30 frames/second image capture capability. The images captured by the camera are processed by the frame grabber and are stored in a personal computer. The IMAQ Vision Builder controls the camera functions, handles the post-processing of the captured images, and performs the measurement of the positions for both the slider and the stator. The camera is installed vertically 20-cm above the oscillating platform, as shown in Fig. 5, to minimize the measurement error. Two halogen illuminators are used as light-enhancing sources.

The camera is used to record the positions of both the slider and the stator over time to determine their velocities and accelerations. The data are then filtered to provide smooth velocity and acceleration time histories. The instantaneous COF is computed from (1) after deriving the acceleration of the slider.

#### IV. SYSTEM OPTIMIZATION

There are several sources of error in the measurement system such as blur, jitter, noise, and lens aberration. It is necessary to optimize the measurement system so that these errors can be reduced to a minimum and the measured results are reliable. Before all the adjustment and optimization, a metric is needed to evaluate the reduction in error quantitatively. The errors are quantified by a tracking mark on either the slider or the stator, as shown in Fig. 6. The width of the mark is  $w$ . The distance from either edge of the mark to a reference point (or line) determines the absolute position of the slider (or stator).

The width  $w$  is constant over time. However, due to blurs, jitters, and other errors, the observed  $w$  varies with the position of the slider (or stator). Let the distance between the reference to the left edge in Fig. 6 be  $x_1(t)$ , and the distance to the right edge be  $x_2(t)$ . If  $n$  positions of the slider (or stator) are recorded during a specific time interval, the average width between these two edges is

$$w_{\text{ave}} = \frac{1}{n} \sum_{j=1}^n (x_2(t_j) - x_1(t_j)). \quad (2)$$

The error of the width  $w$  at  $t = t_i$  is

$$e_p(t_i) = x_2(t_i) - (x_1(t_i) + w_{\text{ave}}). \quad (3)$$

The deviation  $\Delta x_p$  will be

$$\Delta x_p = 12[\text{Max}(e_p(t)) - \text{Min}(e_p(t))]. \quad (4)$$

Therefore, the position error is

$$e_{\text{position}}(\%) = \frac{2 \cdot \Delta x_p}{w_{\text{ave}}} \cdot 100. \quad (5)$$

Assume the tracking mark shifts to the right at  $t_{i+1}$ . The distance between the reference to the left edge at  $t_{i+1}$  is  $x_1(t_{i+1})$ , and the distance to the right edge is  $x_2(t_{i+1})$ . Let the time difference between  $t_i$  and  $t_{i+1}$  be  $T$  (seconds), and let the shutter speed of the camera be  $t$  (seconds). The velocity of the slider (or stator) at  $t = t_{i+1}$  will be

$$V(t_{i+1}) = \frac{[x_1(t_{i+1}) \pm \Delta x_p] - [x_1(t_i) \pm \Delta x_p]}{T \pm t}. \quad (6)$$

The maximum measured velocity is

$$V_{\text{max}}(t_{i+1}) = \frac{x_1(t_{i+1}) + 2\Delta x_p - x_1(t_i)}{T - t} \quad (7)$$

whereas the minimum velocity is

$$V_{\text{min}}(t_{i+1}) = \frac{x_1(t_{i+1}) - 2\Delta x_p - x_1(t_i)}{T + t}. \quad (8)$$

The average velocity difference  $V_{d\text{-ave}}$  is

$$V_{d\text{-ave}} = \frac{1}{n} \sum_{j=2}^n [V_{\text{max}}(t_j) - V_{\text{min}}(t_j)]. \quad (9)$$

The error of the velocity at  $t = t_i$  is

$$e_v(t_i) = V_{\text{max}}(t_i) - [V_{\text{min}}(t_i) + V_{d\text{-ave}}]. \quad (10)$$

The deviation  $\Delta x_v$  will be

$$\Delta x_v = 12[\text{Max}(e_v(t)) - \text{Min}(e_v(t))] \quad (11)$$

and, therefore, the velocity error is

$$e_{\text{velocity}}(\%) = \frac{2 \cdot \Delta x_v}{V_{d\text{-ave}}} \cdot 100. \quad (12)$$

The maximum and the minimum acceleration of the slider (or stator) can be expressed as

$$A_{\text{max}}(t_{i+2}) = \frac{V(t_{i+2}) + 2\Delta x_v - V(t_{i+1})}{T - t} \quad (13)$$

and

$$A_{\text{min}}(t_{i+2}) = \frac{V(t_{i+2}) - 2\Delta x_v - V(t_{i+1})}{T + t}. \quad (14)$$

The average acceleration difference  $A_{d\text{-ave}}$  is

$$A_{d\text{-ave}} = \frac{1}{n} \sum_{j=3}^n [A_{\text{max}}(t_j) - A_{\text{min}}(t_j)]. \quad (15)$$

The error of the acceleration at  $t = t_i$  is

$$e_a(t_i) = A_{\text{max}}(t_i) - [A_{\text{min}}(t_i) + A_{d\text{-ave}}]. \quad (16)$$

The deviation  $\Delta x_a$  will be

$$\Delta x_a = 12[\text{Max}(e_a(t)) - \text{Min}(e_a(t))] \quad (17)$$

and, therefore, the acceleration error is

$$e_{\text{acceleration}}(\%) = \frac{2 \cdot \Delta x_a}{A_{d\text{-ave}}} \cdot 100. \quad (18)$$

The position error in (5) will be utilized as an indicator to evaluate the measurement error during the optimization process. The acceleration error in (18) will be the error in the COF results since the COF is derived from the acceleration of the slider in (1).

Several techniques have been applied to reduce the measurement error. The first one is the tracking mark on the slider/stator and the position detection technique. The original tracking mark

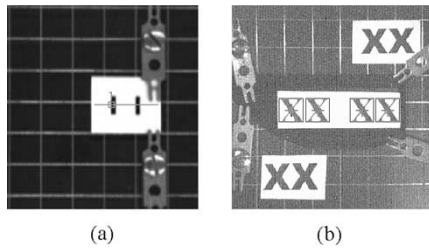


Fig. 7. (a) Tracking mark “I” and (b) tracking mark “X.”

 TABLE II  
 OPTIMIZATION OF POSITION ERROR

conditions	Stationary Platform		motor speed	Oscillating Platform	
	$\Delta x/w$	$\epsilon_{\text{position}}$ (%)		$\Delta x/w$	$\epsilon_{\text{position}}$ (%)
1.mark: I	0.2/1.4 (mm)	28.5	60rpm	0.21/1.32	31.8
			90rpm	0.21/1.31	32.0
			120rpm	0.21/1.32	31.8
2.mark: X	1.2/53.5 (pixels)	4.5	60rpm	1.2/53.6	4.5
			90rpm	1.3/53.7	4.8
			120rpm	1.3/53.6	4.9
3.mark: X (with light)	1.0/53.9 (pixels)	3.7	60rpm	1.0/53.8	3.7
			90rpm	0.9/53.7	3.6
			120rpm	1.1/53.7	4.1
4.mark: X (with light) (calibrated)	0.5/38.7 (pixels)	2.6	60rpm	0.7/38.6	3.6
			90rpm	0.6/38.6	3.1
			120rpm	0.6/38.6	3.1
5.mark: X (with light) (calibrated) (3-order filter)	0.38/38.7 (pixels)	2.0	60rpm	0.49/38.6	2.6
			90rpm	0.4/38.57	2.0
			120rpm	0.49/38.6	2.6

was “I” shaped and the positions of the slider/stator were defined by detecting one single point on the edge of the “I” mark, as shown in Fig. 7(a). The measurement error is around 30%, as seen in the first condition in Table II. The “I” mark was replaced by the “X” mark. The positions of slider/stator are now defined by the central spot of the “X,” which are detected by using a “pattern matching” function in IMAQ [Fig. 7(b)]. Since the “pattern matching” function needs to compare multipoints of the “X” mark to define its center, the results of the position detection is improved and the measurement error is now 4.5% to 4.9% in the second condition in Table II.

In each image captured by the CCD camera, there is a region between the black mark and the white background that the light intensity raises gradually from its (black) low value to its (white) high value. This “gray” region makes the edge of the mark blur and, therefore, introduces errors into the position detection. By tuning down the diaphragm of the camera and applying enhanced lighting on the mark, the contrast between black and white can be improved. The blur at the edge of the mark is reduced and so is the measurement error. This is shown in the third condition of Table II. The error is 3.6% to 4.1% combined with applications of the “X” mark and the extra light.

Due to the nonplanar shape of the lens itself, the image has more distortion when it moves away from the center of the lens. This can be observed in Fig. 8(a). The straight lines, away from the center of the image, have more curvature than those

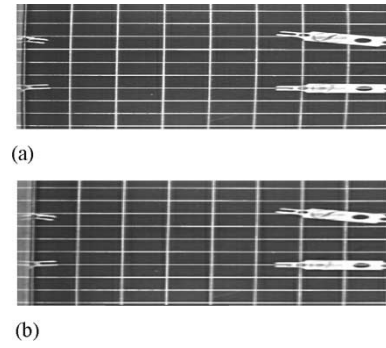


Fig. 8. (a) Grid image before software calibration and (b) grid image after software calibration. The pictures are stretched in width to visualize the curvature of vertical lines.

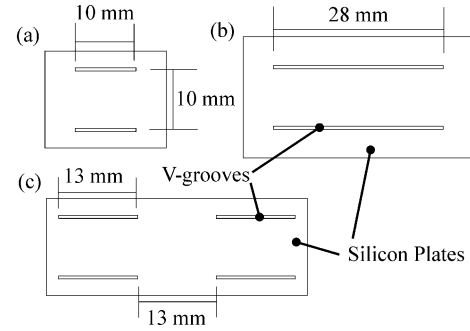


Fig. 9. Schematic top view of stator and slider with microball bearings shown as white bars (a) stator/slider with continuous V-grooves, (b) stator with longer continuous V-grooves, and (c) slider with two-segment V-grooves.

near the center. The “grid calibration” function in IMAQ Vision Builder is developed to deal with this kind of error due to optics. Fig. 8(b) shows the calibrated result. It can be seen that all the grid lines are straight, no matter how far they are from the center of the image. The measurement error is 2.6% to 3.6% in the fourth condition in Table II.

The CCD camera is capable of capturing at most 30 images/second. Any signal with a frequency higher than 30 Hz in the measurement data is unrelated to the real position of the mark and should be filtered out. A third-order filter is designed and tested by using the filter design and analysis tool in MATLAB software. The results are shown in the fifth condition in Table II. By applying the “X” mark, the extra light, the software calibration, and the third-order filter, the measurement error has been dramatically reduced to a range of 2.0% to 2.6%, while the original measurement error was around 30%.

## V. EXPERIMENT RESULTS

Two different designs of the microball bearing are studied using the experiment system described above. The first design has continuous V-grooves, which are 10 mm in length, on both the slider and the stator plates. A schematic top view of one of the plates is shown in Fig. 9(a). The mass of the slider is 0.4 g. A total of 18 microballs are positioned separately in each V-groove. The second design has longer V-grooves, 28 mm in length, on the stator [Fig. 9(b)], while each V-groove on the slider has two segments that are 13 mm in length, as shown in Fig. 9(c). There is a 13-mm space between the two segments.

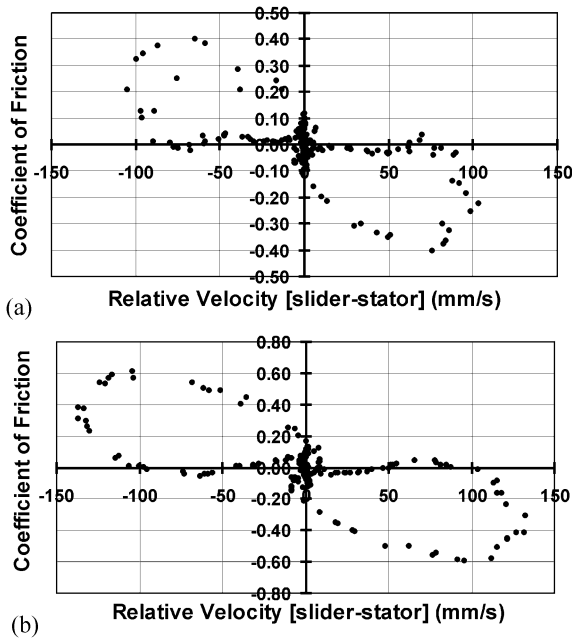


Fig. 10. Results of COF versus relative velocity for microball bearings with short continuous V-grooves on both the stator and the slider at motor speed of (a) 90 rpm and (b) 120 rpm.

Two microballs are positioned in each V-groove in the stator (so one per groove in the slider) and are separated by the space in the slider. The mass of the slider is 0.9 g. The microballs are positioned equidistant away from the end-walls of the V-grooves and the stroke of the oscillating platform is shortened to ensure there is no collision either between microballs themselves or between the microballs and the end-walls of the V-grooves during the experiment. All measurements are performed in steady room environment at a temperature of 27 °C and a relative humidity of 40%RH.

Fig. 10 shows the COF versus relative velocity (the velocity difference between the slider and the stator) for the first design of microball bearings at two motor speeds, 90 and 120 rpm. The static COF (the COF when relative velocity = 0) is 0.1 and the dynamic COF ranges from 0 to 0.6. Since only the microballs are in contact with the slider, the scattered data of dynamic COF are suspected to be due to the collisions either between microballs themselves or between the microballs and the end-walls of the V-grooves. Furthermore, the existing moisture in the measurement environment can alter the silicon surface chemistry and morphology during operation and contribute to the scattered data of the dynamic COF.

Fig. 11 shows the COF result for the second design of microball bearings at two motor speeds, 90 and 120 rpm. The static COF is 0.01 and the dynamic COF ranges from 0.006 to 0.01. Compared to the first microball bearing (multiple balls in one short V-groove), the new microball bearing (single ball in each long V-groove) exhibits only one tenth of both static and dynamic COF. The microball bearing has substantial improvement in frictional behavior provided collisions between microballs themselves or between the microballs and the end-walls of the V-grooves are eliminated. There is still a scattered data observed in the dynamic COF, which is attributed to the presence of moisture in the test environment.

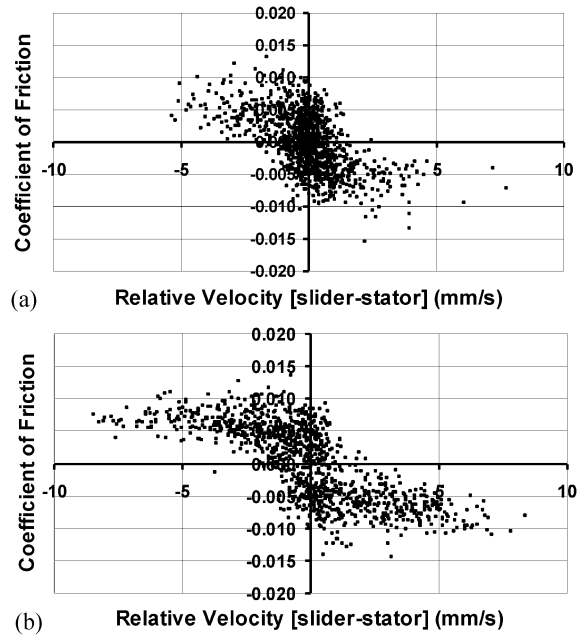


Fig. 11. Results of COF versus relative velocity for microball bearings with long continuous V-grooves on the stator and segmented V-grooves on the slider at motor speed of (a) 90 rpm and (b) 120 rpm.

It is well known that there is a substantial correlation between the surface roughness of interacting surfaces and the COF. The surface roughness of the microballs according to Table I is less than 25 nm. The surface roughness of the V-groove walls was measured using a high-magnification optical microscope equipped with interference differential contrast analyzer (which allows visualizing surface morphology), a 620 focused-ion beam system (FEI, Hillsboro, OR), and a Wyko NT1100 optical profiler (Veeco Instruments, Woodbury, NY). The local average surface roughness was found to be less than 50 nm. However, shallow pits as deep as 200 nm and hillock as big as a few micrometers were observed on the surface of the wall. We believe that the frictional behavior of the test samples will most probably be dominated by the hillocks in this case, although more investigation is needed to understand the influence of the surface roughness on the measured COF. In addition, the method introduced in this paper is applicable to a wide variety of microball bearings regardless of the surface roughness.

## VI. EFFECT OF LOADING

Different weights are added on top of the slider to study the effect of the normal load on COF. The COF is measured with motor speed at 120 rpm. Three measurements are made at each weight and the results are averaged. Fig. 12 shows the measurement results. The static COF at no load (0 g) is 0.01 and the dynamic COF is 0.007. A rapid jump in COF is observed with 1 g load, where the static COF becomes 0.05 and the dynamic COF becomes 0.03. Afterward, the static COF slightly increases from 0.05 (1 g) to 0.07 (40 g) and the dynamic COF increases from 0.03 (1 g) to 0.045 (40 g). It is suggested that the low COF at no load is due to flatness imperfections. Not all microballs are in contact with the slider and the stator. A small amount of load

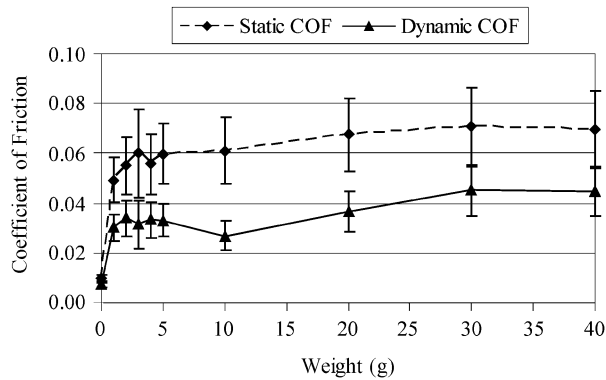


Fig. 12. COF results with different weights on slider. Motor speed is 120 rpm. A rapid increase of COF can be seen from 0 to 1 g.

can bend the slider or the stator slightly, bringing more balls into contact. This can change the COF.

## VII. CONCLUSION

This paper presents an *in-situ* noncontact experimental system to examine the frictional characteristics of microball bearings. This is the first experimental approach proposed to study rolling friction dynamics on the microscale. The system provides controllable motion, with position and velocity to within 2% of desired that is difficult to achieve using MEMS actuators. In addition, a vision system is used that allows the determination of microball bearing COF without any external force interference. The methodology presented in this paper provides a useful template to study the dynamical behavior of linear microball bearings with variety of materials, geometries, and surface qualities.

The effect of collisions between microballs themselves or between the microballs and the end-walls of the V-grooves are studied by using two different designs of microball bearings. It is shown that the collisions increase the friction of the microball bearing. The average static COF for the microball bearing (without collisions) is 0.01 (no load) to 0.07 (40 g), and the dynamic COF is 0.007 (no load) to 0.045 (40 g). Compared to the measured COF for silicon, which ranges from 0.01 to 0.08 [22]–[25] (without weight), the microball bearing has demonstrated its low friction characteristics and is expected to have wide applications in low friction MEMS.

We have demonstrated that it is possible to measure dynamic friction behavior by observing and filtering the forced motion of a slider and a stator through a noncontact vision system. The current measurement system can be further optimized to improve the utility of this experiment in the future. The range of experimental results is basically limited by two factors: 1) the speed and resolution of the camera and 2) the speed and smoothness of the applied motion. Hence, there is tremendous room for improvement: camera speeds go up to thousands of Hertz; the vision resolution is, at the end, limited by available optics which is limited by the wavelength of light. Careful engineering design could lead to macro or micro sliding platforms that operate smoothly at much higher frequencies.

## ACKNOWLEDGMENT

The authors would like to thank D. Wendland for contributions to the development of the LabVIEW program for this project, W.-H. Chuang for his assistance with reviewing the manuscript, and T. C. Loughran and N. A. Ballew for their help with microfabrication processes.

## REFERENCES

- [1] L.-S. Fan, Y.-C. Tai, and R. S. Muller, "IC-processed electrostatic micromotors," in *Technical Digest IEEE Int. Electron Devices Meeting*, New York, 1988, pp. 666–669.
- [2] M. Mehregany, P. Nagarkar, S. D. Senturia, and J. H. Lang, "Operation of microfabricated harmonic and ordinary side-drive motors," in *Proc. 3rd Annu. IEEE Microelectromechanical Systems Workshop*, New York, 1990, pp. 1–8.
- [3] M. Mehregany, S. D. Senturia, and J. H. Lang, "Friction and wear in microfabricated harmonic side-drive motors," in *Tech. Dig. IEEE Solid-State Sensor and Actuator Workshop*, New York, 1990, pp. 17–22.
- [4] D. M. Tanner, N. F. Smith, L. W. Irwin, W. P. Eaton, K. S. Helgesen, J. J. Clement, W. M. Miller, J. A. Walraven, K. A. Petersen, P. Tangyunyong, M. T. Dugger, and S. L. Miller. (2000). "MEMS reliability: Infrastructures, test structures, experiments, and failure modes," Sandia National Laboratories, Albuquerque, NM. [Online]. Available: <http://mems.sandia.gov/search/micromachine/docs/000091o.pdf>
- [5] W. M. van Spengen, "MEMS reliability from a failure mechanisms perspective," *Microelectron. Rel.*, vol. 47, pp. 1049–1060, 2003.
- [6] R. Müller-Fiedler and V. Knoblauch, "Reliability aspects of microsensors and micromechatronic actuators for automotive applications," *Microelectron. Rel.*, vol. 47, pp. 1085–1097, 2003.
- [7] M. Mehregany, K. J. Gabriel, and W. S. N. Trimmer, "Integrated fabrication of polysilicon mechanisms," *IEEE Trans. Electron Devices*, vol. 35, pp. 719–723, June 1988.
- [8] L.-S. Fan, Y.-C. Tai, and R. S. Muller, "Integrated movable micromechanical structures for sensors and actuators," *IEEE Trans. Electron Devices*, vol. 35, pp. 724–730, June 1988.
- [9] S. C. Jacobsen, R. H. Price, J. E. Wood, T. H. Rytting, and M. Rafaelef, "The wobble motor: An electrostatic, planetary-armature microactuator," in *Proc. 2nd Annu. IEEE Microelectromechanical Systems Workshop*, New York, 1989, pp. 17–24.
- [10] H. Fujita, A. Omokada, M. Sakata, and Y. Hatazawa, "Variable gap electrostatic actuators," in *Proc. 8th Sensor Symp.*, Tokyo, Japan, 1989, pp. 145–148.
- [11] S. Kumar and D. Cho, "A proposal for electrically levitating micromotors," *Sens. Actuators A*, vol. 24, pp. 141–149, 1990.
- [12] L. G. Fréchet, S. F. Nagle, R. Ghodssi, S. D. Umans, M. A. Schmidt, and J. H. Lang, "An electrostatic induction micromotor supported on gas-lubricated bearings," in *Proc. 14th Annu. IEEE Int. Conf. Microelectromechanical Systems*, Piscataway, NJ, 2001, pp. 290–293.
- [13] R. Ghodssi, D. D. Denton, A. A. Seireg, and B. Howland, "Rolling friction in a linear microstructure," *J. Vac. Sci. Technol. A*, vol. 11, pp. 803–807, 1993.
- [14] J. A. Ruan and B. Bhushan, "Atomic-scale friction measurements using friction force microscopy: Part I—General principles and new measurement techniques," *J. Tribology*, vol. 116, pp. 378–388, 1994.
- [15] B. Bhushan and V. N. Koinkar, "Tribological studies of silicon for magnetic recording applications," *J. Appl. Phys.*, vol. 75, pp. 5741–5746, 1994.
- [16] —, "Microtribological studies of doped single-crystal silicon and polysilicon films for MEMS devices," *Sens. Actuators A*, vol. 57, pp. 91–102, 1996.
- [17] V. N. Koinkar and B. Bhushan, "Microtribological studies of unlubricated and lubricated surfaces using atomic force/friction force microscopy," *J. Vac. Sci. Technol. A*, vol. 14, pp. 2378–2391, 1996.
- [18] B. Bhushan, J. N. Israelachvili, and U. Landman, "Nanotribology: Friction, wear and lubrication at the atomic scale," *Nature*, vol. 374, pp. 607–616, 1995.
- [19] B. Bhushan, "Micro/nanotribology using atomic force microscopy/friction force microscopy: State of the art," *Proc. Inst. Mech. Eng.*, vol. 212, pp. 1–18, 1998.
- [20] B. Bhushan and C. Dandavate, "Thin-film friction and adhesion studies using atomic force microscopy," *J. Appl. Phys.*, vol. 87, pp. 1201–1210, 2000.

- [21] S. Sundararajan and B. Bhushan, "Static friction and surface roughness studies of surface micromachined electrostatic micromotors using an atomic force/friction force microscope," *J. Vac. Sci. Technol. A*, vol. 19, pp. 1777–1785, 2001.
- [22] K. Noguchi, H. Fujita, M. Suzuki, and N. Yoshimura, "The measurement of friction on micromechatronics elements," in *Proc. 4th Annu. IEEE Microelectromechanical Systems*, New York, 1991, pp. 148–153.
- [23] K. Deng, W. H. Ko, and G. M. Michal, "A preliminary study on friction measurements in MEMS," in *Dig. Tech. Papers Int. Conf. Solid-State Sensors and Actuators*, New York, 1991, pp. 213–216.
- [24] S. Bair, I. Green, and B. Bhushan, "Measurements of asperity temperatures of a read/write head slider bearing in hard magnetic recording disks," *J. Tribology*, vol. 113, pp. 547–54, 1991.
- [25] S. P. M. Cann and H. A. Spikes, "In lubro studies of lubricants in EHD contacts using FTIR absorption spectroscopy," *Tribology Trans.*, vol. 34, pp. 248–56, 1991.
- [26] K. Deng and W. H. Ko, "A study of static friction between silicon and silicon compounds," *J. Micromech. Microeng.*, vol. 2, pp. 14–20, 1992.
- [27] B. K. Gupta, J. Chevallier, and B. Bhushan, "Tribology of ion bombarded silicon for micromechanical applications," *J. Tribology*, vol. 115, pp. 392–399, 1993.
- [28] Q. Chen and G. P. Carman, "Microscale tribology (friction) measurement and influence of crystal orientation and fabrication process," in *Proc. IEEE 13th Annu. Int. Conf. Microelectromechanical Systems*, Piscataway, NJ, 2000, pp. 657–661.
- [29] R. Prasad, N. Macdonald, and D. Taylor, "Micro-instrumentation for tribological measurement," in *Dig. Tech. Papers Int. Conf. Solid-State Sensors and Actuators*, vol. II, Stockholm, Sweden, 1995, pp. 52–55.
- [30] N. R. Tas, C. Gui, and M. Elwenspoek, "Static friction in elastic adhesive MEMS contacts, models and experiment," in *Proc. IEEE 13th Annu. Int. Conf. Microelectromechanical Systems*, Piscataway, NJ, 2000, pp. 193–198.
- [31] J. M. Redmond, M. P. de Boer, and T. A. Michalske, "Integrated modeling and testing of a micro hinged structure for sliding friction measurement," in *Proc. Microelectromechanical Systems*, vol. 66, New York, 1998, pp. 305–311.
- [32] M. P. de Boer, J. M. Redmond, and T. A. Michalske, "A hinged-pad test structure for sliding friction measurement in micromachining," *Proc. SPIE*, vol. 3512, pp. 241–50, 1998.
- [33] S. L. Miller, J. J. Sniogowski, G. LaVigne, and P. J. McWhorter, "Friction in surface micromachined microengines," *Proc. SPIE*, pp. 197–204, 1996.
- [34] I. L. Singer, "Friction and energy dissipation on the atomic scale: A review," *J. Vac. Sci. Technol. A*, vol. 12, pp. 2605–2616, 1994.
- [35] A. Bosseboeuf and S. Petitgrand, "Characterization of the static and dynamic behavior of M(O)EMS by optical techniques: Status and trend," *J. Micromech. Microeng.*, vol. 13, pp. S23–S33, 2003.
- [36] L. Yang and P. Coulborne, "Digital laser microinfrrometer and its applications," *Opt. Eng.*, vol. 42, pp. 1417–1426, 2003.
- [37] M. N. Horenstein, J. A. Perrault, and T. G. Bifano, "Differential capacitive position sensor for planar MEMS structures with vertical motion," *Sens. Actuators A*, vol. 80, pp. 53–61, 2000.
- [38] M. J. Madou, *Fundamentals of Microfabrication*, 2nd ed. Boca Raton, FL: CRC, 2002, pp. 214–215.



**Ta-Wei Lin** was born in Taipei, Taiwan, R.O.C., in 1972. He received the B.S. and M.S. degrees in mechanical engineering from National Taiwan University, Taipei, Taiwan, in 1994 and 1996, respectively, and the M.S. degree in electrical engineering from the University of Maryland (UMD), College Park, in 2001.

From January 2000 to July 2002, he was a member of MEMS Sensors and Actuators Laboratory (MSAL), Department of Electrical and Computer Engineering, UMD. His research involved

the study of microtribology of microball bearings for MEMS applications. Since July 2002, he has been with Asia Pacific Microsystems, Inc., Hsinchu, Taiwan, as a MEMS Engineer, focusing on the area of RF MEMS components development.



University of Maryland (UMD), College Park.

He joined the MEMS Sensors and Actuators Laboratory (MSAL), Department of Electrical and Computer Engineering, UMD, in August 2000. His research is focused on development of power microelectromechanical devices such as electric micromotors and microgenerators using microball bearing technology and spin-on low-k dielectric polymers.

Mr. Modafe is a member of the American Vacuum Society (AVS) and the Materials Research Society (MRS), and an associate member of Sigma Xi. He was awarded the 2002 Spring MEMS Alliance Workshop Best Poster Award and the 2002 AVS Graduate Research Award.



**Benjamin Shapiro** was born in Jerusalem, Israel, in 1973. He received the B.S. degree in aerospace engineering from the Georgia Institute of Technology, Atlanta, in 1995 and the Ph.D. degree in control and dynamical systems from the California Institute of Technology, Pasadena, in 1999. His Ph.D. thesis was focused on fluid dynamics and symmetry breaking in jet engines.

He joined the Department of Aerospace Engineering at the University of Maryland (UMD), College Park, as an Assistant Professor in 2000.

His current research interests include modeling and control of microfluidic motion through applied electric fields, modeling and design of multichannel microfluidic networks driven via surface tension, and experimental identification of friction dynamics on the microscale. He is part of the interdisciplinary Small Smart Systems Center, UMD. He has a number of collaborations with outside MEMS groups, and is part of the modeling and design MEMS efforts at Nanostream, Inc., the University of California, Los Angeles, and the National Institute of Standards and Technology, Gaithersburg, MD. He also organizes the Minta Martin seminar series in the Department of Aerospace Engineering, UMD.



**Reza Ghodssi** (S'92–M'97) was born in Tehran, Iran, in 1966. He received the B.S., M.S., and Ph.D. degrees in electrical engineering from the University of Wisconsin, Madison, in 1990, 1992, and 1996, respectively. His Ph.D. thesis was focused on development of a high-aspect ratio microfabrication process for an electrostatic-driven MEMS device using X-ray lithography and LIGA technology.

He was a Postdoctoral Associate and a Research Scientist with the Microsystems Technology Laboratories and the Gas Turbine Laboratory at the Massachusetts Institute of Technology (MIT), Cambridge, from 1997 to 1999. During his tenure at MIT, he developed the building-block MEMS fabrication technologies for a microturbine generator device and also served as an Assistant Director on that project. In January 2000, he joined the Department of Electrical and Computer Engineering and the Institute for Systems Research, University of Maryland (UMD), College Park, as an Assistant Professor. His research interests are in the design and development of microfabrication technologies and their applications to microsensors, microactuators, and integrative microsystems.

Dr. Ghodssi is a Cofounder of the MEMS Alliance Group in the greater Washington area and a member of the AVS and MRS. He has served as a program Cochairman for the 2001 International Semiconductor Device Research Symposium (ISDRS) and, since 2002, as a Chairman of the MEMS and NEMS Technical Group at the American Vacuum Society (AVS). He was awarded the 2001 UMD George Corcoran Award, the 2002 National Science Foundation CAREER Award, and the 2003 UMD Outstanding Systems Engineering Faculty Award.